Development and verification of fast reactor burnup calculation module FRBurner in code system CBZ

Junshuang Fan[1]*, Go Chiba[1].

[1]*Division of Applied Quantum Science and Engineering, Faculty of Engineering, Hokkaido University, Kita 13 Nishi 8, Kita-ku, Sapporo, 060-8628, Japan*

CBZ is a general-purpose reactor physics analysis code system, and FRBurner, which focuses on fast reactor burnup calculations, was developed recently with diverse combinations of available methodologies. Verification of this module is conducted with the OECD/NEA fast rector benchmark since this benchmark provides various types of fast reactors. Four key reactor physics parameters, effective neutron multiplication factor k_{eff}, effective delayed neutron fraction β_{eff}, sodium void reactivity $\Delta\rho_{\text{void}}$ and Doppler reactivity $\Delta\rho_{\text{Doppler}}$ are the focus and compared to two references provided by JAEA and CEA, respectively. The biases between the results from FRBurner and the JAEA and CEA references on each of the above key parameters are less than 0.5%, 1%, 3% and 7%, and less than 1.0%, 4%, 12%, and 12%, respectively. The comparison indicates that the FRBurner module would provide acceptable results for general-type fast reactor physics analysis in research. As one innovation, the detailed burnup chain model, which is significantly different from a generally-used pseudo fission product model in fast reactor neutronic analysis, is applied in FRBurner. The detailed burnup chain model helps FRBurner explicitly provide information about the inventory of fission products for nuclear waste management and spent fuel reprocessing.

Keywords: fast reactor, burnup, verification, methodology

*Corresponding author. Email: fanjsh@eng.hokudai.ac.jp

1. Introduction

Neutronics calculation methods have been well established by a number of studies over past decades, and there are two main directions in the neutronics calculation field: the deterministic and Monte Carlo methods. FRBurner has been developed as a fast reactor burnup calculation module in the CBZ code system[1], which is a deterministic code under development at Hokkaido University. While the fast reactor calculation code systems REBUS[2], ERANOS[3] and MARBLE[4] exist, the need for a particular code system that enables diverse purpose (accuracy) calculations still exists for our recent and future works. For instance, it is desirable to use an identical code for both preliminary design calculation with a low-resource-cost option and final parameter confirmation calculation with a high-accuracy option so that consistency is maintained between calculations and computing resources are saved. Moreover, the demand for a new algorithm, cross-section library, burnup chain model, etc., exists for our current and future works. It is difficult to meet such flexible demands without a self-developed code system. For instance, one original point of this work is the detailed burnup chain model calculation that is becoming available in FRBurner. The detailed burnup chain model calculation significantly differs from the pseudo fission product method that is generally used. It can provide essential information on inventory or spent fuel composition which may be useful in nuclear waste management. One instance of the detailed burnup chain model calculation is introduced in this paper to demonstrate the availability of the FRBurner burnup computing function. To apply such a new study method is one important purpose of this work; thus, developing an independent fast reactor calculation code system is necessary.

One primary task for FRBurner is showing its capacity to provide satisfactory results through comprehensive verification work. Consequently, one OECD/NEA fast neutronic analysis benchmark[5] was chosen for the verification work. Four sodium-cooled fast reactor cores which contain three types of fuel, metallic fuel, MOX fuel and carbide fuel, are

provided in this report. In addition, two of these cores are large-sized with a thermal power of 3,600 MWth, and the others are middle-sized with a thermal power of 1,000 MWth. The diversity on core type provides adequate universality, increasing the reliability of this verification work.

From the perspective of practical application, it is beneficial to understand the differences among methodologies of a module, such as FRBurner, that has diverse calculation methodology options. Thus, the differences in (i.e., effects on) numerical results while applying a zero-dimensional/one-dimensional/two-dimensional lattice model, diffusion/transport theory for whole-core calculations and coarse/fine-energy group structure cross-section library are investigated in this work. This impact investigation would help potential users to choose an appropriate methodology for diverse purposes, and section 4 of this paper is devoted to concluding this investigation.

The introduction of the FRBurner module for the basic theory and numerical method are given in section 2. The verification work based on the bias comparison is described in section 3. The impact of the methodology options on numerical results is discussed in section 4, and the numerical examples of burnup calculation with a detailed chain model are shown in section 5.

2. Basic theory and numerical method

2.1. Multi-group library and its generation procedure

The FRBurner module uses a multi-group cross-section library called CBZLIB to calculate problem-dependent medium-wise multi-group (or effective) cross sections. CBZLIB consists of the infinite dilution cross sections, the scattering matrices with an arbitrary order of the Legendre expansion, and the self-shielding factors for the reactions of (n,n), (n,f) and (n,γ). The self-shielding factors for the elastic removal cross sections and for the current-weighted total cross sections are also included.

These multi-group library data are obtained from the ENDF-formatted evaluated nuclear data files and the 'point-wise (resonance-reconstructed) ENDF' (PENDF) files with the NJOY-99 code[6] through the processing sequence of the BROADR, PURR, GROUPR and MATXSR modules. In the GROUPR module, the narrow resonance approximation is adopted, and the IWT=8 weighting function, which is adaptive for fast reactor study is chosen for multi-group constants calculation. The generated text files in the MATXS format are converted into the other text files in a specific format readable by CBZ. The PENDF files are generated by the FRENDY code developed at JAEA[7]. In the present work, we generate several multi-group libraries with different numbers of energy groups from several evaluated nuclear data libraries.

2.2. Fuel assembly calculations to obtain homogeneous (homogenized) cross sections

Since all the assemblies are treated as homogeneous in the whole-core calculations by FRBurner, spatial homogenization for the assemblies is required prior to whole-core calculations. This is done at the assembly calculation step. In the assembly calculation of FRBurner, all assemblies including blanket assemblies are modeled with a single assembly with the reflective boundary conditions, and multi-group cross section calculations (or resonance self-shielding calculations) and neutron flux spatial distribution calculations are conducted with this single assembly model.

Regarding the assembly model, three options can be chosen: the zero-dimensional model, the one-dimensional cylinder model and the two-dimensional hexagonal model as shown in **Figure 1**.

In the zero-dimensional model, nuclides number densities are spatially averaged over a whole assembly with volume weight, and the resulting homogeneous mixture is treated. The background cross sections for resonance treatment are calculated with this mixture,

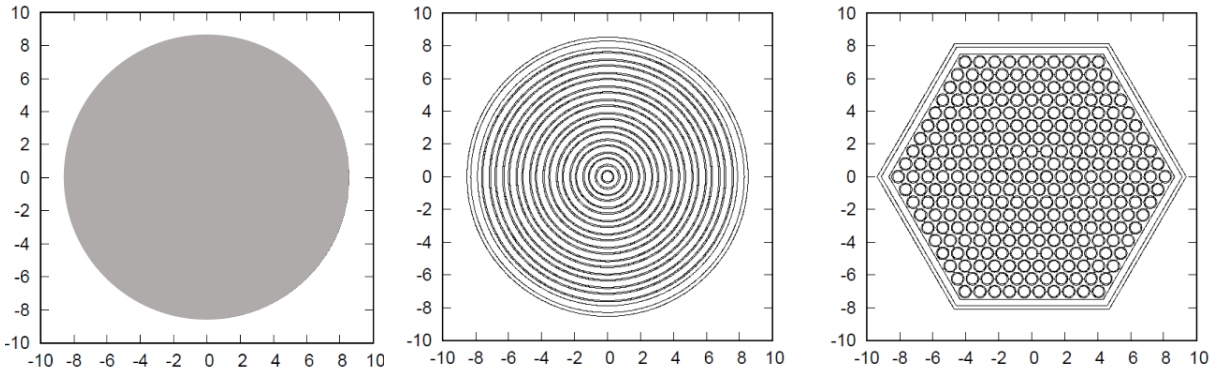

Figure 1 Three options of lattice model for assembly calculation: zero-dimensional, one-dimensional and two-dimensional (left to right).

and the multi-group cross sections of this mixture can be easily calculated. In this case, no spatial neutron flux calculations are required, and the infinite neutron multiplication factor can be easily calculated by solving the one-point B_1 equation.

In the cylinder and hexagonal models, multi-group cross sections of each medium are calculated using the method proposed by Tone[8]. In Tone's method, the lattice heterogeneity effect is taken into account in background cross-section calculations via the collision probabilities. After multi-group cross sections of each medium are obtained, the multi-group neutron transport equation is solved by the collision probability method, and multi-group neutron flux spatial distributions are calculated. The leakage effect is accounted for the pseudo absorption cross sections defined from the critical buckling. With the calculated neutron flux spatial distribution, spatial homogenization is carried out to obtain the homogenized multi-group cross sections The homogenized multi-group cross sections are used in the subsequent whole-core calculations without any group collapsing (or condensation). The homogenized multi-group microscopic cross sections are calculated in the initial burnup cycle, and the homogenized macroscopic cross sections in the subsequent burnup cycles are calculated from these microscopic cross sections and nuclide number densities in the concerned burnup step.

2.3. Whole-core calculations to obtain eigenvalues and neutron flux distributions

Although several solvers for three-dimensional systems have been implemented in CBZ, the present version of FRBurner can only use the two-dimensional cylinder model; thus, users should construct a cylindrical core model from a three-dimensional core configuration. The neutron diffusion or transport equation defined for the cylindrical core model can be solved, and the eigenvalue and the neutron flux spatial distribution over the whole core can be obtained. When the neutron diffusion equation is solved, a solver PLOS, which adopts the finite-volume spatial discretization, is used. When the neutron transport equation is solved, a solver SNRZ, which adopts the diamond-differencing spatial discretization scheme and the discrete ordinates angular discretization scheme, is used. The inner iterations are accelerated by the diffusion synthetic acceleration in SNRZ. Both solvers implement the coarse-mesh finite difference acceleration for the outer power iteration.

Calculations of the reactivity induced by the reduction in coolant density and the increase in the fuel temperature can be calculated by the exact perturbation theory in an arbitrary burnup cycle. The homogenized microscopic cross sections of the assemblies at these perturbed states are conducted in the initial burnup cycle. The effective delayed neutron fraction β_{eff} can be also calculated with the forward and adjoint neutron fluxes obtained by PLOS or SNRZ.

2.4. Fuel burnup calculations

With the neutron flux energy and spatial distribution obtained by the whole-core calculation, the nuclide-wise reaction rates can be calculated, and with these reaction rates, the changes in the nuclide number densities with time can be calculated. This nuclide transmutation process is simulated by fuel burnup calculations with a nuclide burnup chain.

In the nuclide burnup chain, 21 important actinides are considered. On fission products, the pseudo fission products are generally used in the fast reactor neutronic analyses since the variation in neutron capture cross sections of various fission products is not significant in fast reactors. When the pseudo fission products are introduced to a burnup chain, the number of nuclides in the burnup chain could be small, and the fuel burnup calculations can be done easily. On the other hand, the detailed information on the nuclide inventory included in the spent nuclear fuel is required for the works relevant to nuclear waste management or spent fuel reprocessing. In such cases, it is preferred that the fission products are explicitly treated in a burnup chain. This requires a relatively large computer memory since the information on nuclide inventories including a large number of fission products must be stored for all burnup media through whole-core burnup calculations. Such fuel burnup calculations, with the detailed nuclide burnup chain treating fission products explicitly, are also possible in FRBurner.

Nuclides transmutation is represented by the Bateman equation, and the solution to this equation is obtained by the matrix exponential method in FRBurner. There exists several methods to numerically calculate the matrix exponential in CBZ, FRBurner adopts the mini-max polynomial approximation method[9,10]. This can be adopted to the Bateman equation including the quite short half-lived nuclides, which should be considered in burnup calculations with the detailed nuclides burnup chain.

Fuel exchange during multiple burnup cycles can be simulated by FRBurner. Since a reactor core is modeled as a cylinder, the explicit representation of a reactor core consisting of fuel assemblies with different irradiation histories is impossible. In FRBurner, nuclide number densities are calculated for each assembly with its irradiation history, but in the whole-core calculations, the macroscopic cross sections are obtained through the averaged number densities over a region which is involved in burnup calculation.

3. Verification work with the OECD/NEA benchmark

In this section, essential information about four fast reactor cores which are provided by the benchmark, the calculation methodology of FRBurner and the reference results are introduced. Bias comparison and error analysis are discussed also in this section.

3.1. Core configuration

As mentioned in section 1, four fast reactor cores are described in the benchmark: MET-1000, MOX-1000, MOX-3600 and CAR-3600. The name of the cores indicates the fuel type and power level (core size), as listed in **Table 1**. Each core is modeled as multi-layer cylinder model, and the width of each layer is calculated from the sum of the hexagonal-cross-section assembly areas of corresponding layers. The layout of the MET-1000 multi-layer cylinder model is shown in **Figure 2** as one example, the y-axis is the axial direction and the x-axis is the radial direction. Medium information is listed according to the medium number in the right of the figure.

Table 1 Fuel type and core size information of each benchmark core

Core name	Fuel type	Power level [MWe]
MET-1000	Metallic	1000
MOX-1000	MOX	1000
MOX-3600	MOX	3600
CAR-3600	Carbide	3600

The benchmark provides number density data at the beginning of equilibrium cycle (BOEC), and users calculate the number density data at the end of equilibrium cycle (EOEC). The effective neutron multiplication factor k_{eff}, effective delayed neutron fraction β_{eff}, sodium void reactivity $\Delta\rho_{\text{void}}$ and Doppler reactivity $\Delta\rho_{\text{Doppler}}$ are four target parameters, and the reference results provided by a variety of institutes of these four parameters at BOEC and EOEC are given in the benchmark. The condition for calculating $\Delta\rho_{\text{void}}$ is that all sodium is voided. The condition for calculating $\Delta\rho_{\text{Doppler}}$ is that the

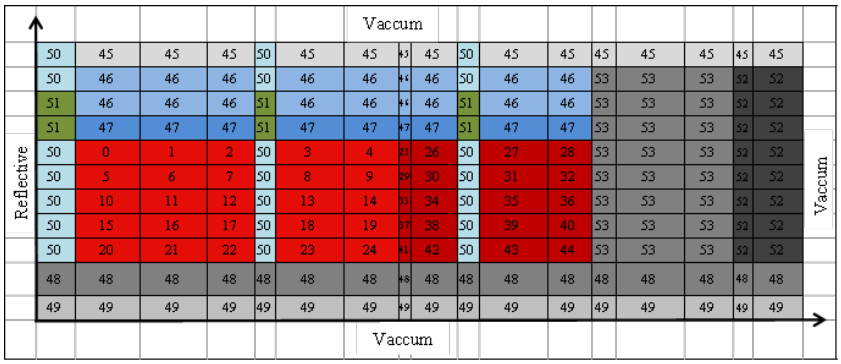

Number	Medium
0∼24	Inner core
25∼44	Outer core
45	Upper structure
46	Gas plenum
47	Replace sodium
48	Lower reflector
49	Lower structure
50	Empty duct
51	Control absorber
52	Shield rod
53	Radial reflector

Figure 2 Multi-layer cylinder model of MET-1000.

temperature in the core regions are changed to twice those of the standard state.

The normalized (scaling to unit length) forward and adjoint neutron fluxes at the center of each core calculated by the diffusion solver with the 70-group cross section are shown in **Figure 3** in order to show the basic characteristics of these four cores. It is obvious that MET-1000 consisting of metallic fuel has a harder neutron spectrum. Energy group wise $\Delta\rho_{\text{void}}$ and $\Delta\rho_{\text{Doppler}}$, which are calculated by the diffusion solver with the 70-group cross section are shown in **Figure 4**, and component-wise $\Delta\rho_{\text{void}}$ is shown in **Figure 5**. From **Figure 4** it is noticed that all four cores have a significant $\Delta\rho_{\text{void}}$ peak around 0.8 MeV, which is caused by the sodium nuclide, and $\Delta\rho_{\text{Doppler}}$ in an energy range higher than 10^5 eV is negligible. Then, **Figure 5** reveals that $\Delta\rho_{\text{void}}$ is mostly caused by the scattering and leakage components.

3.2. Calculation methodology in the verification work

FRBurner applies the traditional two-step method to solve problems. Three lattice model options are available in the lattice calculation procedure: two-dimensional hexagonal rigorous model, one-dimensional cylinder model and zero-dimensional homogeneous model. The heterogeneity of the assembly structure cannot be considered in the whole-core calculation procedure since the whole core is completely homogenized as a two-dimensional

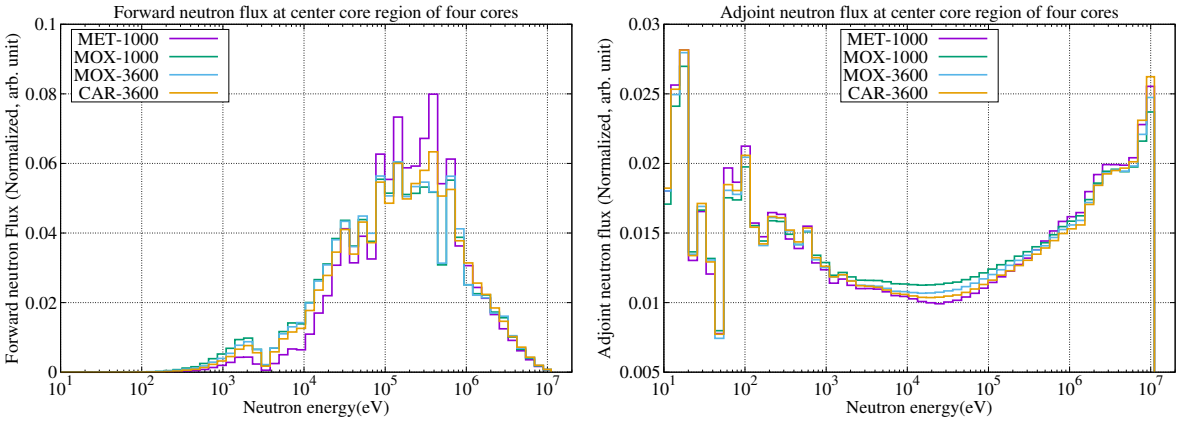

Figure 3 Forward and adjoint neutron fluxes at the center of four cores.

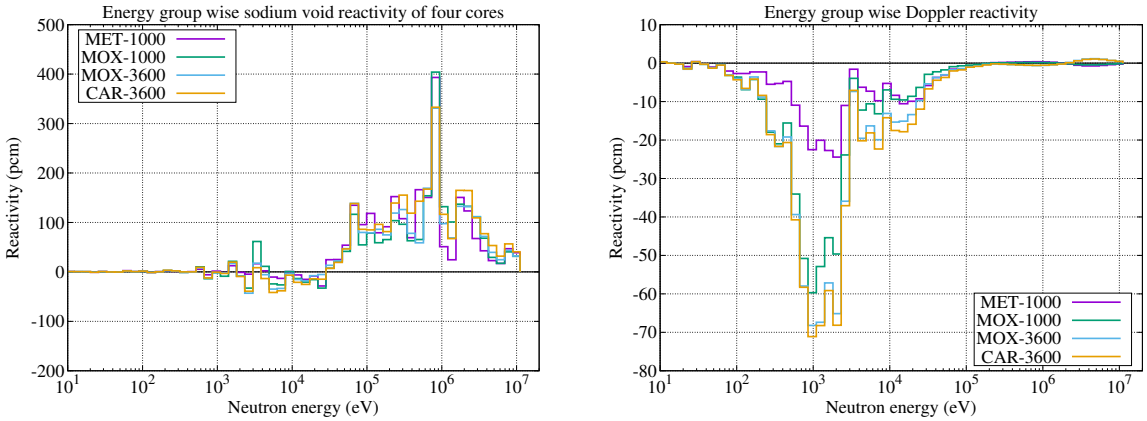

Figure 4 Energy group wise $\Delta\rho_{\mathrm{void}}$ and $\Delta\rho_{\mathrm{Doppler}}$.

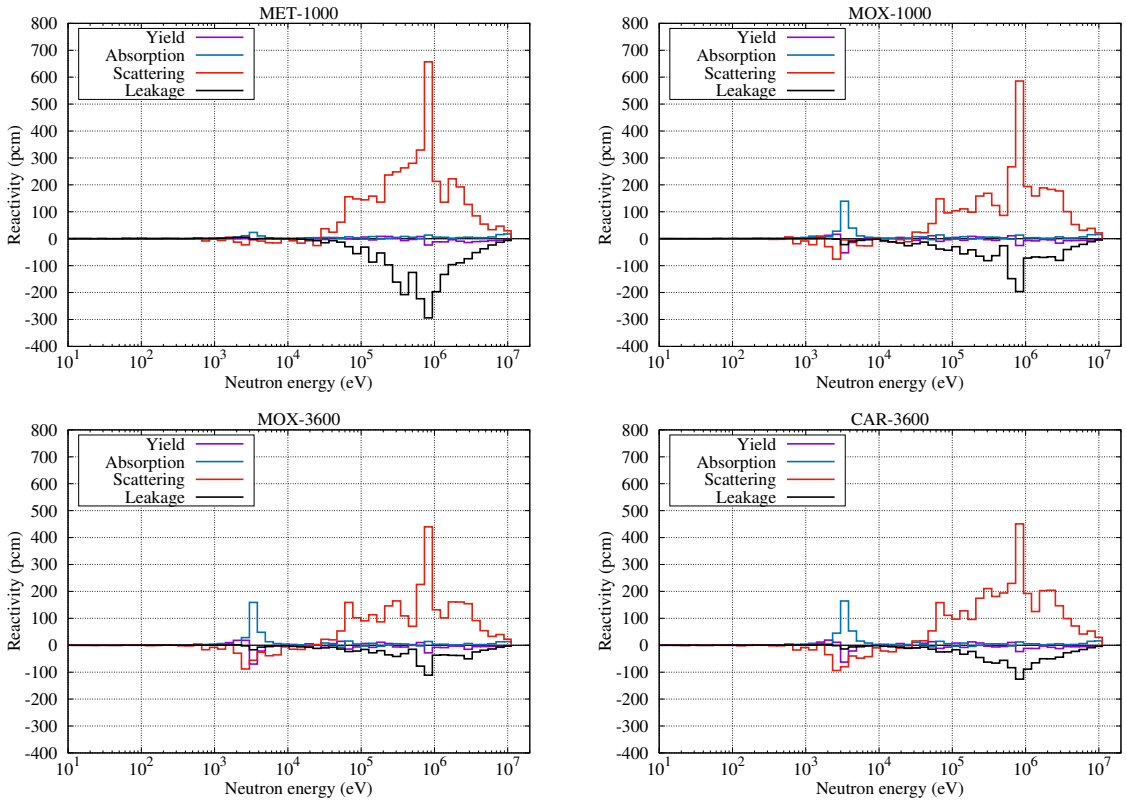

* $\Delta\rho_{\mathrm{void}}$ can be divided into the non-leakage and leakage component wise reactivity. The non-leakage component consists of the yield, absorption and scattering components.

Figure 5 Component wise $\Delta\rho_{\mathrm{void}}{}^{*}$ of four cores.

cylinder. Considering other options for theory, library and energy group structure, therefore, multiple combinations in FRBurner can be chosen for diverse problems according to purpose.

In the verification part, the most rigorous methodology, the two-dimensional lattice model in assembly calculation procedure with the transport theory-based solver SNRZ (P_1S_4) with 280-group CBZLIB, was used. The 280-group structure CBZLIB is based on the JAERI fast set-3 (JFS-3) structure proposed for sodium-cooled fast reactor analysis, and each group of this 70-group structure is divided into 4 groups. References provided by JAEA (Japan Atomic Energy Agency) and CEA (Commissariat à l'énergie atomique) were used for verification. The methodologies of these two chosen references are shown in **Table 2**. The suffix of the reference name in **Table 2** is to maintain consistency with the benchmark. It should be noted that these references use 3-dimensional models in the whole-core calculation step. Although these two institutes provided several references, we only chose one reference from each institute. The JENDL-4.0[11]-based CBZLIB and the JEFF-3.1.1[12]-based CBZLIB were used for the present calculation for comparison with the JAEA-2 and CEA-1 reference results, respectively.

To verify the burnup function of FRBurner, the number density at EOEC was calculated by FRBurner based on the BOEC number density which is given by the benchmark.

Table 2 Methodologies used for the references.

	JAEA-2	CEA-1
Library	JENDL-4.0	JEFF-3.1
Lattice code	MARBLE(SLAROM-UF)	ECCO
Core code	MARBLE(TRITAC)	ERANOS VARIANT8
Lattice geometry	Heterogeneous	Heterogeneous
Core geometry	Homogeneous	Homogeneous
Approximation	Diffusion(Transport correction)	Transport SP_3
Depletion chain	-	Pseudo FP
Fuel S/A	One-dimensional multi-ring, 70g-70g	Two-dimensional hexagonal, 1968g-33g
Energy groups in lattice/core	70-group/70-group	1968-group/33-group

As this work was preliminary verification, the criteria of the FRBurner module calculation on k_{eff}, β_{eff}, $\Delta\rho_{\text{void}}$ and $\Delta\rho_{\text{Doppler}}$ were set at 0.5%, 3%, 10% and 10%, respectively.

3.3. Bias comparison with the JAEA reference result

The JAEA-2 reference only contains the results of MET-1000 and MOX-3600. The reference and the FRBurner calculation results are summarized in **Table 3**. A relative biases comparison is shown in **Figure 6**. Relative biases on k_{eff} are multiplied by 10 for clarification.

Table 3 JAEA-2 reference and FRBurner results based on the JENDL-4.0 library.

	BOEC				EOEC				
	k_{eff}	β_{eff}	$\Delta\rho_{\text{void}}$	$\Delta\rho_{\text{Doppler}}$	k_{eff}	β_{eff}	$\Delta\rho_{\text{void}}$	$\Delta\rho_{\text{Doppler}}$	$\Delta\rho_{\text{cycle}}$
JAEA-2									
MET-1000	1.0289	339	2170	-375	1.0081	338	2256	-389	-2004
MOX-3600	1.0133	363	1948	-921	1.0193	355	1977	-881	581
FRBurner									
MET-1000	1.02910	336	2147	-352	1.00815	335	2239	-366	-2019
MOX-3600	1.00889	361	2002	-924	1.01602	353	2027	-878	696

* k_{eff} is unitless parameter, the unit of others are per cent mille (pcm).
* $\Delta\rho_{\text{cycle}}$ value in benchmark is not calculated from k_{eff}. To keep consistency, $\Delta\rho_{\text{cycle}}$ calculated by k_{eff} is listed at here.

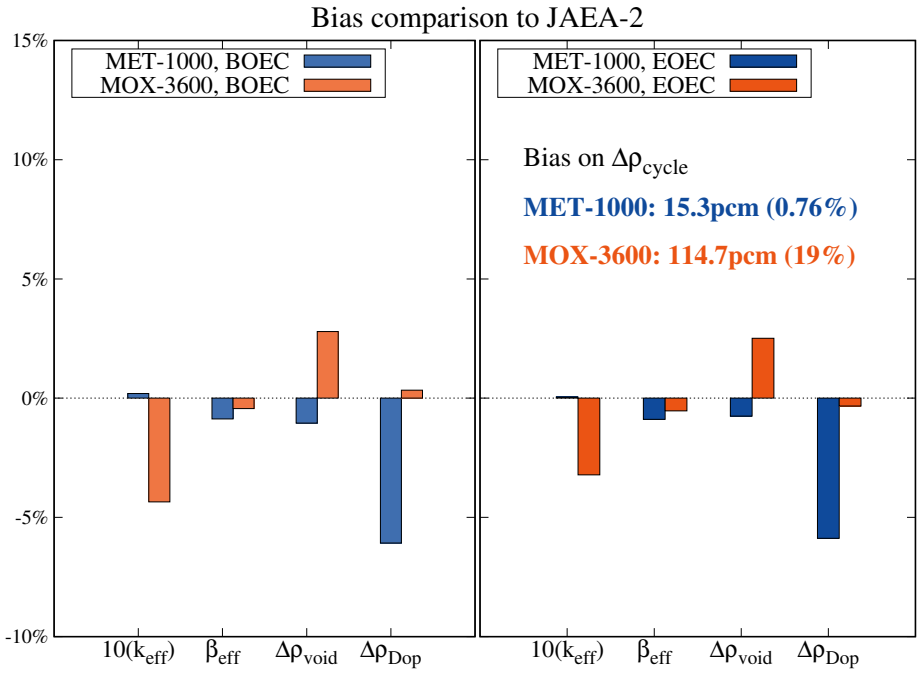

Figure 6 Biases comparison between FRBurner and JAEA-2 reference at BOEC and EOEC.

The maximum bias of each parameter is less than 0.5%, 1%, 3% and 7% respectively. Preferable results were obtained through comparison between the JENDL-4.0-based CB-

ZLIB FRBurner calculation results and the JAEA-2 reference results. The biases at BOEC and EOEC were consistent with each other, suggesting perfect performance of the burnup calculation function.

3.4. Bias comparison with the CEA reference result

The CEA-1 reference was used as supplement although it provides results for all four cores due to methodology differences between CEA-1 and FRBurner. The CEA-1 reference and the FRBurner calculation results are summarized into **Table 4**. Relative biases of each parameter are summarized into **Figure 7**.

Table 4 CEA-1 reference and FRBurner result based on the JEFF-3.1.1 library.

	BOEC				EOEC				
	k_{eff}	β_{eff}	$\Delta\rho_{\mathrm{void}}$	$\Delta\rho_{\mathrm{Doppler}}$	k_{eff}	β_{eff}	$\Delta\rho_{\mathrm{void}}$	$\Delta\rho_{\mathrm{Doppler}}$	$\Delta\rho_{\mathrm{cycle}}$
CEA-1									
MET-1000	1.0372	355	2190	-362	1.0100	354	2385	-357	-2596
MOX-1000	1.0316	345	1922	-789	1.0141	342	2060	-767	-1673
MOX-3600	1.0162	381	1931	-971	1.0136	-	2056	-887	-252
CAR-3600	1.0097	391	2122	-1048	1.0147	381	2233	-949	488
FRBurner									
MET-1000	1.03836	343	2012	-348	1.01553	342	2108	-364	-2165
MOX-1000	1.03792	334	1845	-731	1.02422	332	1881	-747	-1289
MOX-3600	1.01451	370	1856	-926	1.01881	362	1896	-884	413
CAR-3600	1.00903	380	2053	-970	1.02050	371	2162	-921	1281

* k_{eff} is unitless parameter, the unit of others are per cent mille (pcm).
* $\Delta\rho_{\mathrm{cycle}}$ value in benchmark is not calculated from k_{eff}. To keep consistency, $\Delta\rho_{\mathrm{cycle}}$ calculated by k_{eff} is listed at here.

The maximum bias of each parameter is less than 1.0%, 4%, 12% and 12%, respectively. These results are regarded as acceptable regardless of the relatively large biases (>10%) on $\Delta\rho_{\mathrm{void}}$ and $\Delta\rho_{\mathrm{Doppler}}$ because such a large bias does not always occur in all four cores.

3.5. Bias analysis

Firstly, the comparison between the FRBurner calculation and the JAEA-2 reference suggested that FRBurner can give acceptable results on fast reactor analysis work, although consistent results are not obtained when compared with the CEA-1 reference. The

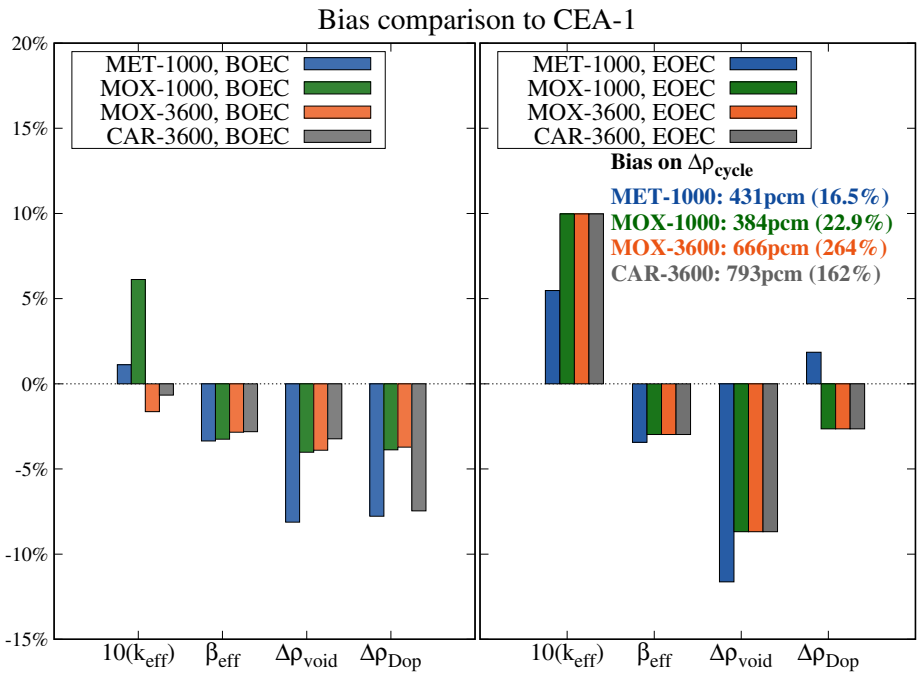

Figure 7 Biases comparison between FRBurner and CEA-1 reference at BOEC and EOEC.

reason for the discrepancy between FRBurner and CEA-1 is differences in calculation conditions. More importantly, the biases at BOEC and EOEC show obvious differences when compared with the CEA-1 reference. This is because the depletion calculation conditions between FRBurner and CEA-1 are different. According to benchmark, the recommended depletion calculation is using Molybdenum to substitute every fission production. So that the discrepancy caused by depletion model between references can be eliminated. We chose the same depletion calculation condition as JAEA-2 reference applies for keeping consistency. CEA-1, however, applies pseudo-FP treatment which is different from recommendation.

As the FRBurner module applies a two-dimensional homogeneous model in the whole-core calculation step, the biases found in the two comparisons should be caused by the difference of models in the whole-core calculation step. It is noteworthy that the impact of this difference in the whole-core calculation step would not be large since acceptable agreement was observed when compared with the JAEA reference result.

Additionally, as for the biases on β_{eff} found in comparison with the CEA-1 reference, the delayed neutron emission data are partly responsible them. While energy-dependent delayed neutron yield, ν_{d}, is used in CBZ, energy-independent ν_{d} is adopted by CEA-1. As ν_{d} becomes smaller with increased incident energy, FRBurner tends to give smaller β_{eff} than the CEA-1 reference.

4. Impact of the methodology option on numerical result

In this section, the differences (effects on) results while applying zero-dimensional/one-dimensional/two-dimensional lattice model, diffusion/transport theory and coarse/fine-energy group structure library are investigated. The dependencies among these three effects are also studied. The differences between two different order options of the transport theory solver ($\text{P}_\text{N}\text{S}_\text{N}$) are studied as supplement. Data used in this section are obtained only from the JEFF-3.1.1-based CBZLIB calculations, because there is no correlation between ENDF library and the terms which are analyzed in this section. Accordingly, the JENDL-4.0-based calculation results are not discussed here. To investigate the differences, we focused not only k_{eff}, β_{eff}, $\Delta\rho_{\text{void}}$ and $\Delta\rho_{\text{Doppler}}$, but also the components of $\Delta\rho_{\text{void}}$: the non-leakage and leakage components, are investigated. To avoid redundancy, only the effects at BOEC are shown in tables and figures in this section since these effects have no relationship with the burnup calculation.

4.1. Three lattice models (model effect)

Three options for the lattice model in the first step of the traditional two-step method are provided in FRBurner. It is essential to recognize the degree of effect caused by the one-dimensional cylinder model/two-dimensional hexagonal model when compared with the zero-dimensional homogeneous model since the zero-dimensional model is applied particularly in the beginning of work, and researchers would like to adjust the core config-

uration based on this preliminary calculation result. It would be beneficial if users could estimate a more accurate value using the result of such comparison.

Firstly, the two-dimensional lattice model effect is shown in **Figure 8**. Specific values of each parameter are recorded into appendix. From **Figure 8** we find that:

(1) The two-dimensional lattice model makes obvious changes on k_{eff}, $\Delta\rho_{\text{void}}$ and $\Delta\rho_{\text{Doppler}}$ approximately from 0.4% to 0.6%, from -5% to -8% and 5%, respectively, compared with the zero-dimensional lattice model.

(2) The lattice model effect does not depend on the theory(diffusion/transport) and the energy group structure.

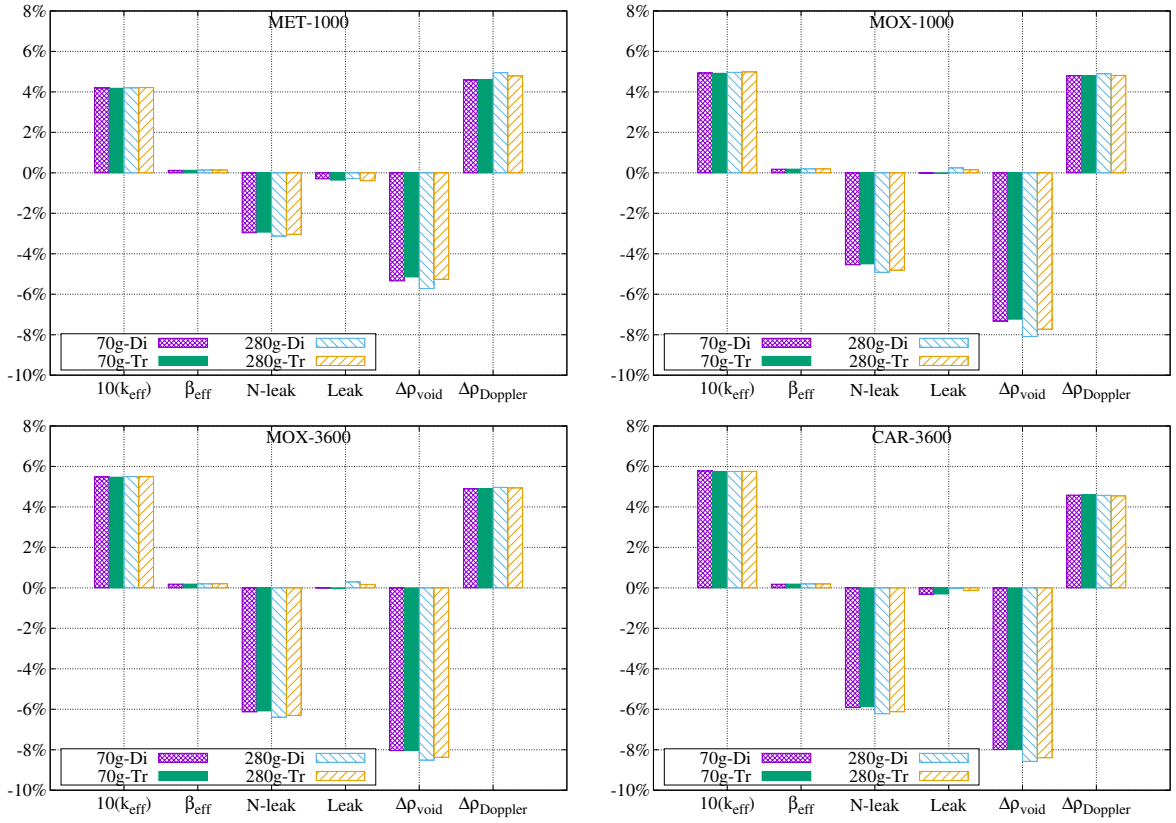

Figure 8 Two-dimensional lattice model effects of multiple methodologies in JEFF-3.1.1-based-CBZLIB calculations.

Secondly, direct comparison between the two- and one-dimensional lattice models is shown in **Figure 9**.

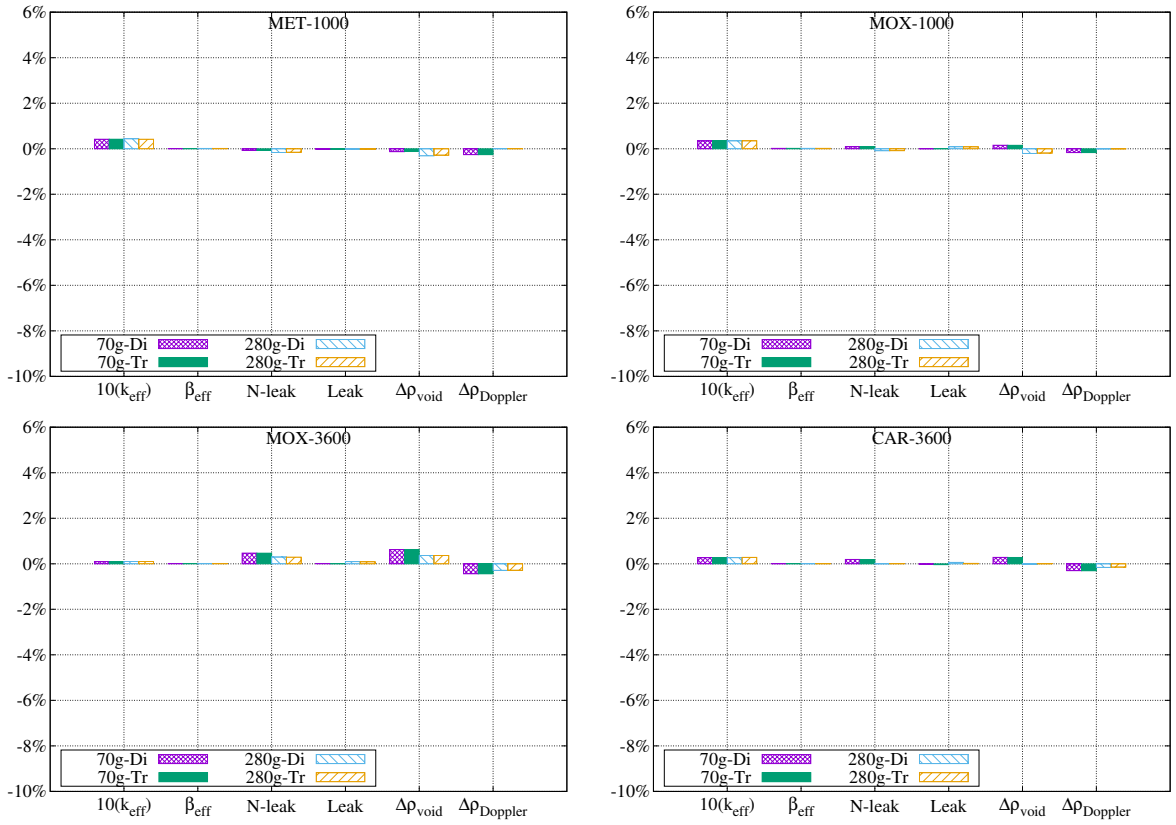

Figure 9 Direct comparison between two-dimensional and one-dimensional lattice models.

According to **Figure 9** we indirectly come to the conclusion that the one-dimensional lattice model causes almost identical changes on four parameters compared with the two-dimensional lattice model; namely, the one-dimensional lattice model represents the characteristics of the two-dimensional hexagonal assembly pretty well.

The increase in k_{eff} obtained from the heterogeneous lattice model is due to the spatial and energy self-shielding effects, which reduces the neutron absorption of the two/one-dimensional lattice model system compared with that in the zero-dimensional lattice. Next, the decrease in $\Delta\rho_{\text{void}}$ is due to the decrease in the non-leakage component of $\Delta\rho_{\text{void}}$ which is positive. More accurately, the decrease in the non-leakage component of $\Delta\rho_{\text{void}}$ is due to the changes in yield, absorption and scattering fractions (the main contribution is the scattering fraction). The sign of yield, absorption and scattering fractions are negative, positive and positive respectively, and the heterogeneous model enhances the yield fraction, and decreases the absorption and scattering fractions. Thus, these total effects decrease $\Delta\rho_{\text{void}}$ when applying the heterogeneous model. Thirdly, the increase in $\Delta\rho_{\text{Doppler}}$ is due to the change in the background cross section Σ_b in resonance calculations. Σ_b in the homogeneous model is larger than that in the heterogeneous model. Therefore, the absorption cross section of ^{238}U and its change due to temperature increase in the homogeneous model is larger than those in the heterogeneous model.

4.2. Two solvers (transport-effect)

At present, FRBurner has three available solvers that apply the diffusion theory, the transport theory and the simplified $-\ \mathrm{P}_3$ (SP_3) method, respectively. In this work, only the diffusion and transport solvers were employed for verification and methodologies differences investigation of the differences in methodologies. The differences between the transport and diffusion theory solvers under three lattice models condition, with two energy group structures are studied in this subsection. **Figure 10** shows the transport-effect

obtained by the six methodologies.

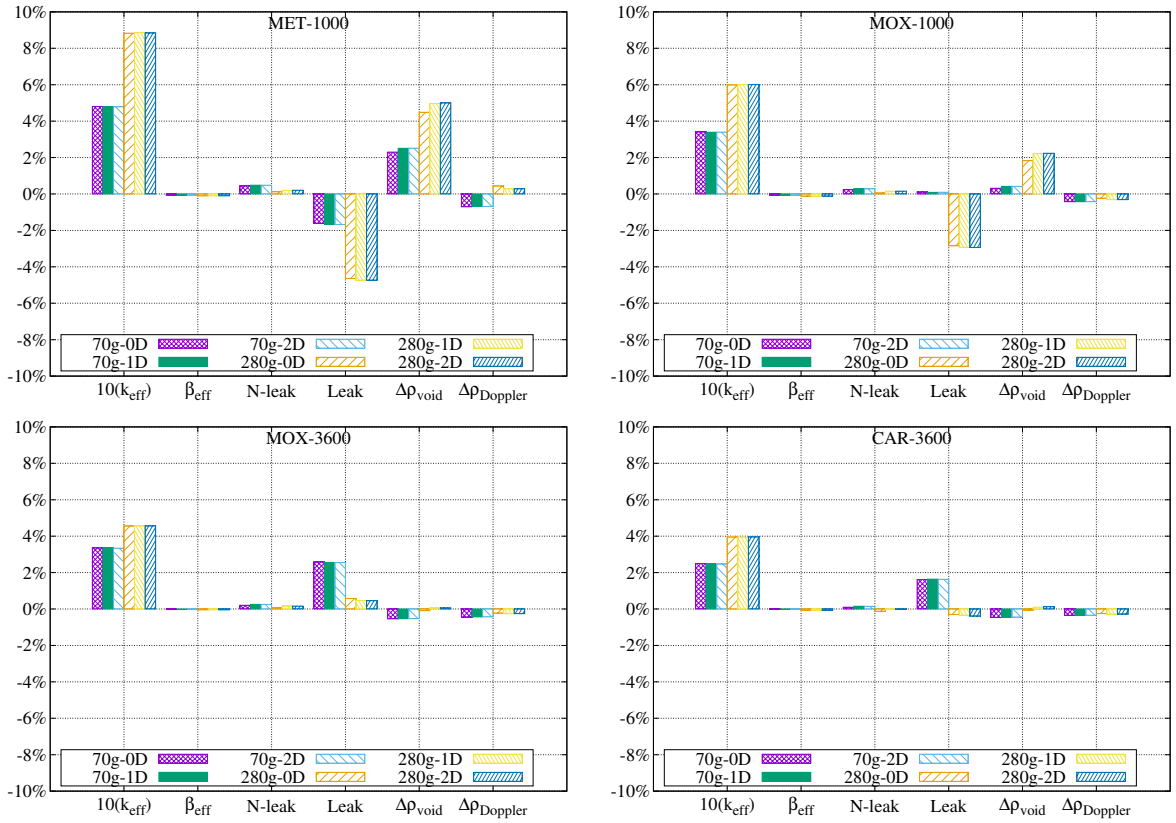

Figure 10 Transport-effect obtained by multiple methodologies in JEFF-3.1.1-based-CBZLIB calculations.

(1) The transport theory solver (transport-effect) causes a significant increase in k_{eff}, about 0.4% for the 70-group calculation and 1.0% for the 280-group calculations.

(2) Concerning $\Delta\rho_{\text{void}}$, the transport-effect differs for different sized cores. The effect on the middle-sized cores is more obvious than that in the large-sized cores. The transport-effect on $\Delta\rho_{\text{void}}$ of the large-sized cores is quite small.

(3) The transport-effect strongly relates to the energy group structure, and fine-energy group structure enhances the transport-effect. However, the transport-effect is independent on the lattice model.

To find out the cause of transport-effect, and why the fine-group structure enhances transport-effect, we take the MET-1000 and MOX-3600 as targets, the neutron flux in

several typical locations, relative difference between transport-solver-calculated ϕ_{Tr} and diffusion-solver-calculated neutron flux ϕ_{Di} (transport-effect on neutron flux), macroscopic total and scattering cross-section and microscopic scattering cross-section of Na and Fe are investigated together. **Figures** 11 and 12 show the energy-wise distribution of transport-effect on neutron flux. For MET-1000, mediums 0, 10 and 20 are in inner-core, mediums 27, 35 and 43 are in outer core. The mediums 0, 10, 20 and medium 27, 35, 43 belong to two fuel assemblies, respectively. The mediums 0 and 27 locate at top, and mediums 20 and 43 locate at bottom. Similarly, for MOX-3600, mediums 0, 18 and 36 belong to inner-core, mediums 47, 57 and 67 are outer core. The mediums 0, 18, 36 and mediums 47, 57, 67 belong to two fuel assemblies, respectively. The mediums 0 and 47 locate at top and mediums 36 and 67 locate at bottom.

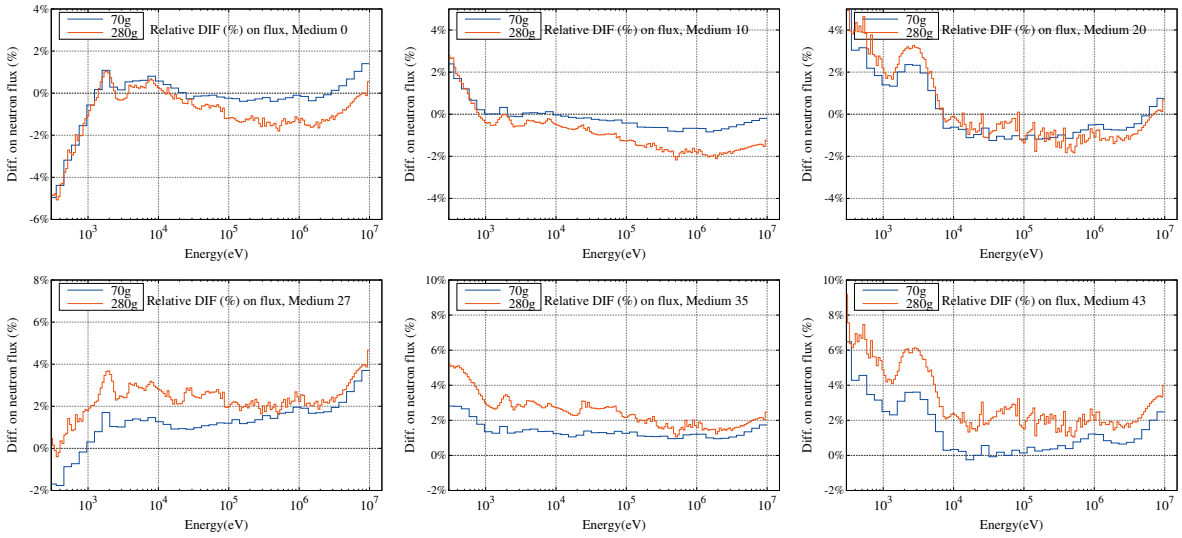

Figure 11 Transport-effect on neutron flux, MET-1000.

The following points can be observed:

- Although transport-effect shows negative effect at some regions and some energy ranges, eventually it is a positive effect for target reactors.
- The transport-effect in outer-core regions and near-reflector regions is more obvious.
- Fine-energy group structure enhances transport-effect at entire energy range, mostly

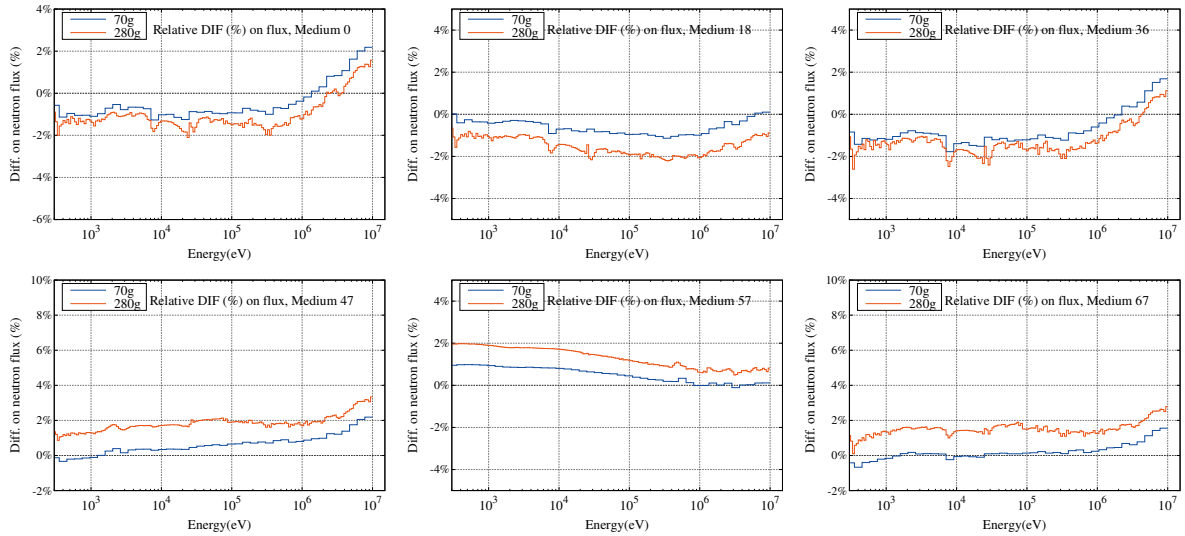

Figure 12 Transport-effect on neutron flux, MOX-3600.

for outer-core regions.

Besides, **Figure 11** suggests that transport-effect has correlation with scattering cross-section since there is a slight peak around 3keV, and Na has a elastic-scattering cross-section peak around 3keV.

The transport-effect on neutron flux behaves differently in inner-core and outer-core regions suggests that it is a "spatial-correlated" effect. The transport-effect reduces inner-core neutron flux level, and increases outer-core neutron flux level. Due to the outer-core region has more fissile material, the k_{eff} is increased eventually. If considering the transport-effect reversely, the nature of transport-effect is the error caused by diffusion approximation. Therefore, above two figures indicates that diffusion-solver increases the neutron flux level in inner-core, and reduces flux level in outer-core. The gradient of neutron flux is increased by using diffusion-solver. Naturally, the neutron leakage is further overestimated due the increased neutron flux gradient.

As for the detailed mechanism of fine-energy group structure enhances the transport-effect, the authors think it is difficult to give a quantified explain since the system is complicated, so that further discussion is omitted at here.

Above discussion also indicates one thing that diffusion-solver shall cause larger error for sodium-cooled reactor, especially for reactor which has multiple regions (inner-region, outer-region). Analysis for such type of reactor system should not be conducted with diffusion-solver. When neutronic analysis of such type of reactor system is conducted by diffusion theory, one should pay more attention on bias caused by diffusion approximation.

Next, the reason for the increase in $\Delta\rho_{\text{void}}$ obtained by the transport solver for the middle-sized cores is the same as that for the increase in k_{eff}. That is, correcting the neutron leakage overestimation would decrease the leakage component of $\Delta\rho_{\text{void}}$, as shown in **Figure 10**. Neutron leakage in large-sized cores, however, is less significant than that in middle-sized cores. Accordingly, correcting the overestimation of neutron leakage for large-sized core calculations does not result in significant differences when compared with the diffusion theory solver. The authors believe that the different levels of neutron leakage for different sized cores are responsible for the difference of this significant transport-effect.

Additionally, the transport-effect calculated for MET-1000 is larger than that for the others. This is due to a relatively harder neutron spectrum of the metallic fuel core than other cores. For this reason, the overestimation of neutron leakage is more significant.

4.3. Coarse/fine energy group structure (fine-energy group effect)

Two energy group structures were applied in this work: 70-group and 280-group. There would be six methodologies for each core: two/one/zero/dimensional lattice model with diffusion/transport theory solver. **Figure 13** shows this fine-energy group effect and indicates that:

(1) The fine-energy group calculation largely increases k_{eff}: around 0.2% for the diffusion theory solver calculations, and from 0.2% to 0.6% for the transport theory solver calculations.

(2) The fine-energy group calculation has a negative effect on $\Delta\rho_{\text{void}}$. The negative ef-

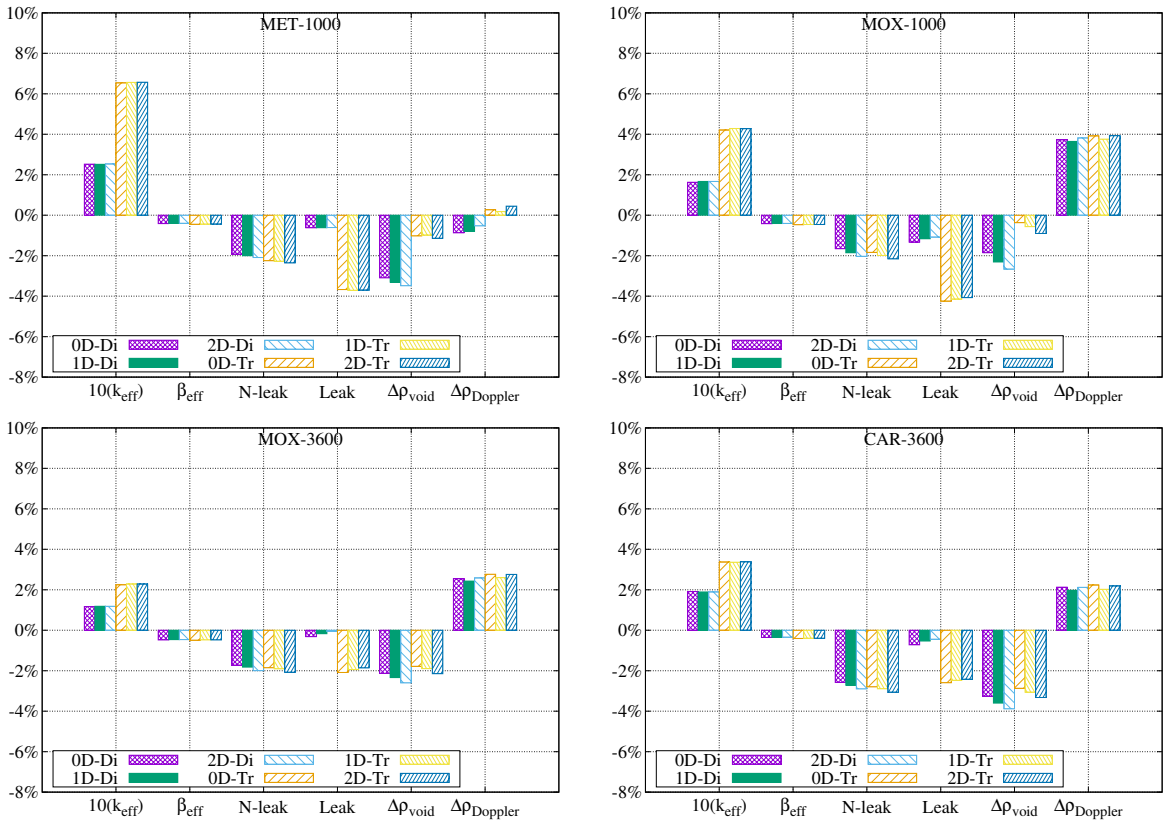

Figure 13 Fine-energy group structure effects under multiple methodologies in JEFF-3.1.1-based-CBZLIB calculations.

fect is due to the decrease of the non-leakage component of $\Delta\rho_{\text{void}}$ (positive value) and the increase of leakage component of $\Delta\rho_{\text{void}}$ (negative value). Besides, the negative effects on $\Delta\rho_{\text{void}}$ differ between the middle-sized and large-sized cores. In the middle-sized cores, the negative effect is more intense in the diffusion theory solver calculations; however, in the large-sized cores, the negative effect is nearly identical.

(3) The fine-energy group effect is independent of the lattice model, but it has a relationship with the calculation theory. For large-sized cores, the difference between theories becomes negligible.

There are several possible explanations for these fine-energy group effects. The first is the weighting function used to generate the multi-group constant. In this study the IWT=8 weighting function was used. In the 70-group case the IWT=8 weighting function may have caused errors, but the errors would be reduced in the 280-group structure case. The second is the change in the resonance absorption cross sections of medium mass nuclei such as Fe and Na. These two factors should contribute to the fine-energy group effect.

4.4. The order of transport solver

In FRBurner, the order of the transport solver is determined by two parameters: P_N and S_N, which are the maximum order of the Legendre polynomial for the anisotropic scattering cross section expansion, and the number of discrete points in a direction angle, respectively. Generally, option P_1S_4 is applied. P_3S_8 is known to be more accurate; however, it could be extremely time-consuming. **Figure 14** shows the differences between the P_1S_4 and P_3S_8 options in 70-group calculations.

Option P_1S_4 could provide preferable results with enough accuracy for problems such as preliminary/initial stage calculation that do not require high accuracy.

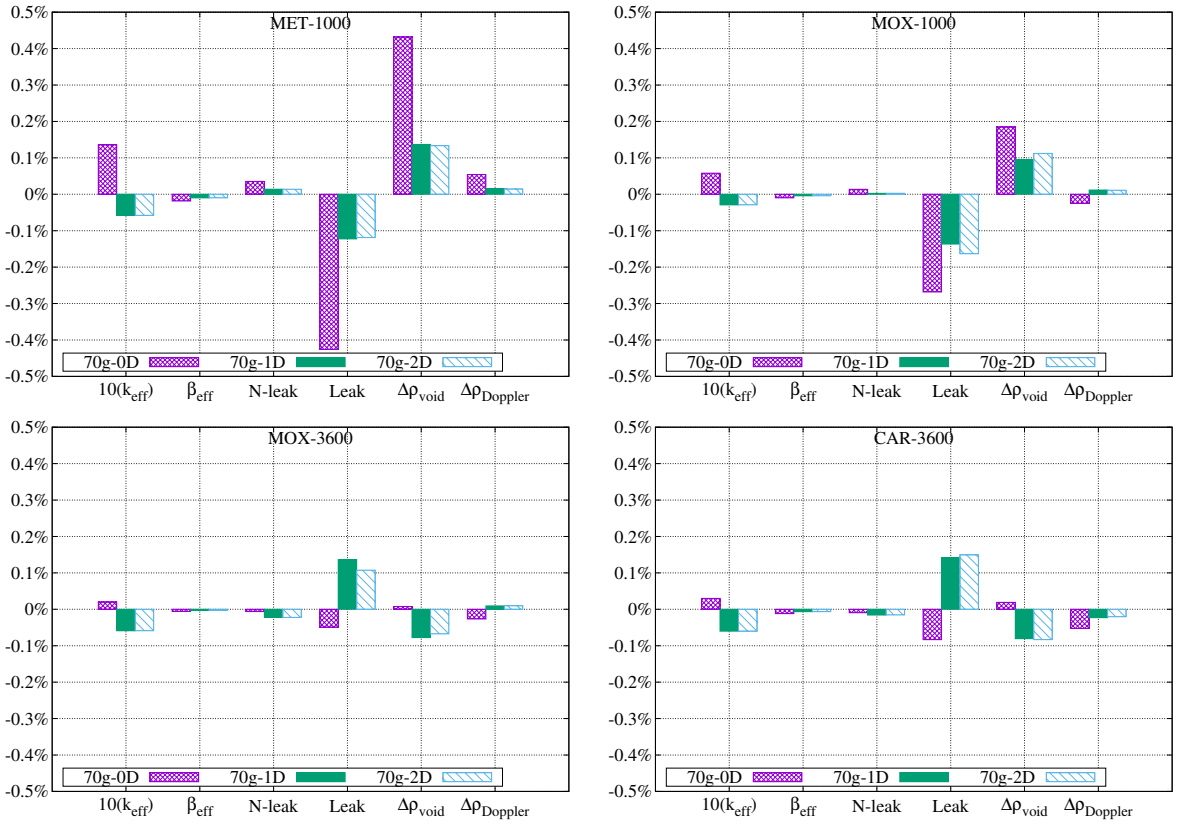

Figure 14 Differences between P_1S_4 and P_3S_8 options for transport solver.

4.5. Dependency among three variables on methodology

The above investigations have thoroughly described the degree to which changes would be caused by different methodologies. The dependencies among the lattice model effect, transport-effect and fine-energy group effect are discussed in this subsection.

Firstly, from **Figure 8** it is obvious that the lattice model effect has no relationship with the core calculation theory and the energy group structure. This independence indicates that users could freely choose any lattice model according to need. On the contrary, it is clear from **Figure 10** that the transport-effect depends on the energy group structure. As discussed above, we already know that it is not appropriate to apply the fine-energy group option with the diffusion theory. Accordingly, the fine-energy group effect has s relationship with the calculation theory as well, as shown in **Figure 13**.

The dependency investigation suggests users how to properly set the calculation methodology with the FRBurner module.

5. Examples of burnup calculation results with the detailed nuclides chain model

In this section, some examples of burnup calculation results with the detailed nuclides chain model that explicitly treats the fission products are presented. The target fast reactor is JSFR-1500, which is a 1,500 MWe large MOX-fueled sodium-cooled fast reactor developed by JAEA through a feasibility study on the commercialized fast reactor cycle systems[13]. This reactor has been designed to achieve a long operation period and a high conversion ratio. JSFR-1500 has two different core concepts: the transition-phase core and the equilibrium core, and the latter was treated in the present calculation. Detailed calculation conditions such as material compositions and geometrical configurations were taken from the open literature. The cylindrical core model of JSFR-1500 prepared for FRBurner is shown in **Figure 15**.

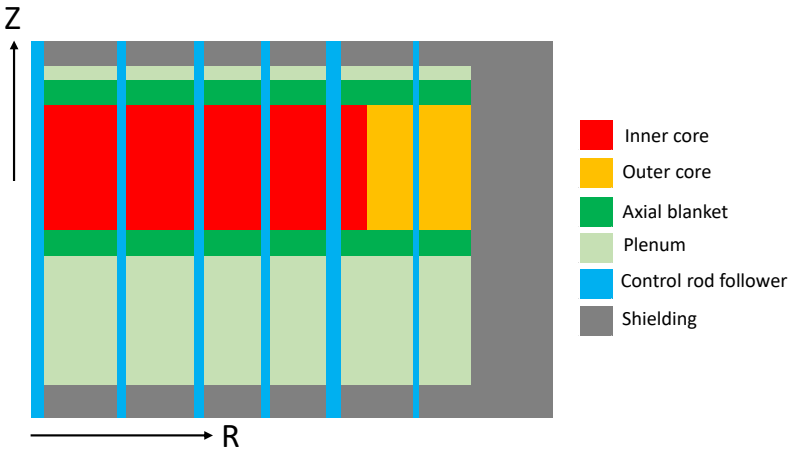

Figure 15 JSFR-1500 Cylindrical core model for FRBurner calculation.

In the present calculations, the JENDL-4.0-based 70-group CBZLIB was used, and the zero-dimensional homogeneous assembly model and the diffusion theory-based solver PLOS were adopted. For the burnup calculations, a detailed nuclide chain model consisting of 193 fission products, which are included in the most detailed nuclide chain model used in the SRAC-2k6 code[14], and four other nuclides, was used. That is a total of 197 nuclides were explicitly treated in this detailed chain model. The calculated effective neutron multiplication factor k_{eff} during the initial six burnup cycles is shown in **Figure 16**. Since the number of refueling batches is four for all the assemblies, the core reaches the equilibrium state after the initial three cycles. At the end of the equilibrium cycle, k_{eff} is slightly larger than unity. This suggests that our calculation model is reasonable.

5.1. Direct calculations of back-end-related quantities

Through whole-core burnup calculations with the detailed burnup chain model, precise information on the compositions of discharged fuel assemblies per cycle can be obtained; and important quantities related to the back-end nuclear fuel cycle, such as the radioactivity and the decay heat of the discharged nuclear fuel can be calculated. This is one of the specific features of FRBurner, and this cannot be accomplished if the conventional simple chain model including the pseudo fission products is used.

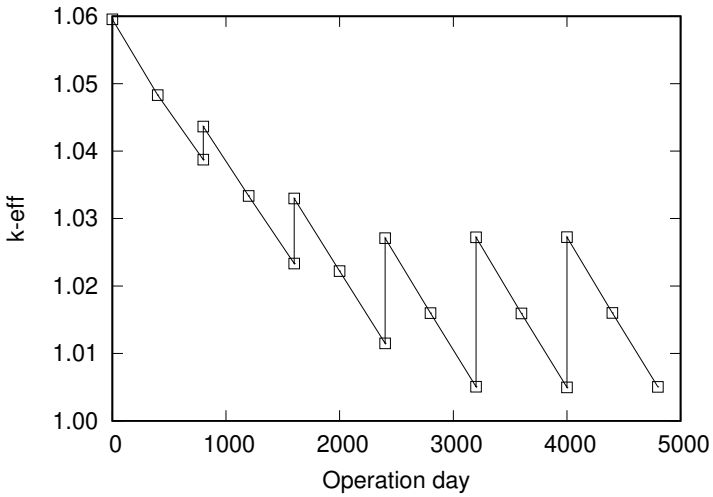

Figure 16 Effective neutron multiplication factor during burnup

Figure 17 shows the radioactivity and the decay heat of the fuel discharged after a cooling period following an equilibrium cycle. This figure also provides the contributions of heavy metal and fission products separately. Additionally, it is also possible to show the nuclide-wise contributions. Note that the nuclear fuel cooling calculations were performed by the Cooler module of the CBZ code system, and all the fission products defined in JENDL/FPY-2011[15,16] are explicitly take into consideration.

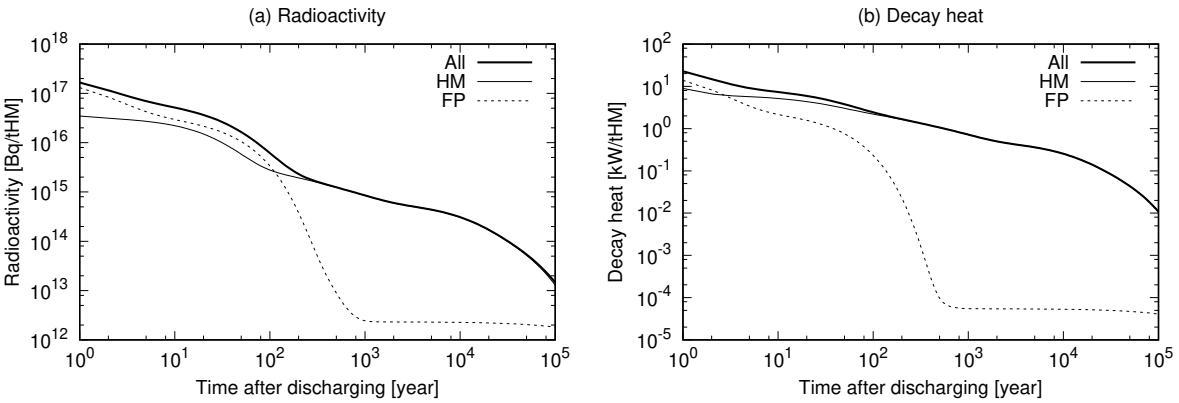

Figure 17 Radioactivity and decay heat of discharged nuclear fuel.

5.2. Quantification of impact of impurities in recycled fuel on neutronics parameters

In the nuclear fuel cycle, certain reusable materials such as fissile (or fissionable) nuclides are extracted from discharged fuels in spent fuel reprocessing. During this process, a small fraction of other materials should accompany the reusable materials, and the accompanying materials should be considered as impurities in the recycled fuel. Since burning the minor actinides is also an important role of the fast reactors, the minor actinides are also extracted in the reprocessing. However, since it is well known that chemical separation of the minor actinides from the rare earth elements is a challenge, special measures to achieve high separation efficiency are required. Under this circumstances, the concept of a fast reactor with poorly-decontaminated fuel has been proposed to enhance the feasibility of the nuclear fuel cycle[17]. In this type of work, the impact of the impurities in the recycled fuel on the neutronic properties of fast reactors should be quantified. This cannot be addressed by the conventional fast reactor burnup calculations with a simple burnup chain model including the pseudo fission product methods. On the other hand, this can easily be done by FRBurner with the detailed chain model mentioned below.

Here we assume that the rare earth elements are mixed in the recycled fuel at a fixed volume ratio. Note that yttrium is also considered as one rare earth element because of its chemical similarity to the rare earth elements. Since we need to obtain the compositions of the rare earth elements in the recycled fuel in the equilibrium state, iterative calculations are performed to obtain converged compositions of the rare earth elements. The plutonium enrichment in the charged fuels is adjusted so as to make k_{eff} at the end of the equilibrium state close to unity. The volumetric ratios of each rare earth element to the total in the discharged fuel in the equilibrium state with different volume fractions of the rare earth element to the recycled fuel are shown in **Figure 18**. The dependence of the volumetric ratios on the volume fractions is generally small, but slight dependence is observed in

some rare earth elements such as Gd and Pm. This kind of evaluation cannot be done easily when the conventional simple burnup chain model is employed.

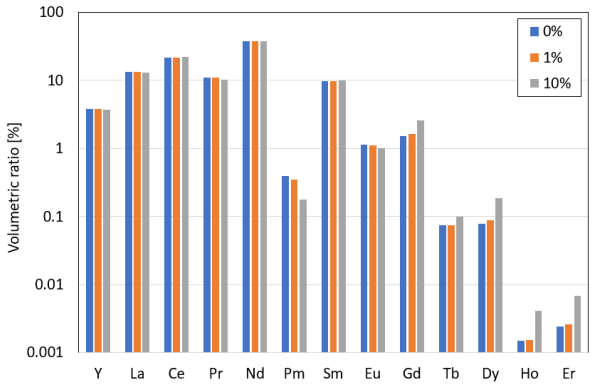

Figure 18 Volumetric ratio of each rare earth element in discharged fuel.

The impact of the impurities in the recycled fuel on several neutronic parameters is quantified in **Figure 19**. The changes in neutronic parameters by adding the rare earth elements to the recycled fuel are consistent with the previous work[17].

6. Conclusion

FRBurner, a recent developed fast reactor neutronic calculation module of the CBZ code system, has been verified through the solving of four fast reactor core problems and compared with two references which are provided by two institutes. Four reactor physics key parameters were focused in this verification: k_{eff}, β_{eff}, $\Delta\rho_{\text{void}}$ and $\Delta\rho_{\text{Doppler}}$. The maximum biases obatined from the JENDL-4.0-based CBZLIB and JEFF-3.1.1-based CBZLIB were less than 0.5%, 1%, 3% and 10%, and 1.0%, 4%, 12% and 12%, respectively. This verification work indicated that FRBurner could provide accurate prediction on k_{eff}, β_{eff}, $\Delta\rho_{\text{void}}$ and $\Delta\rho_{\text{Doppler}}$ for general-type fast reactor systems due to the four fast reactor cores which were used for verification cover typical fuel types and core sizes proposed as fast reactor concepts.

Secondly, the authors analyzed the differences between methodologies that are avail-

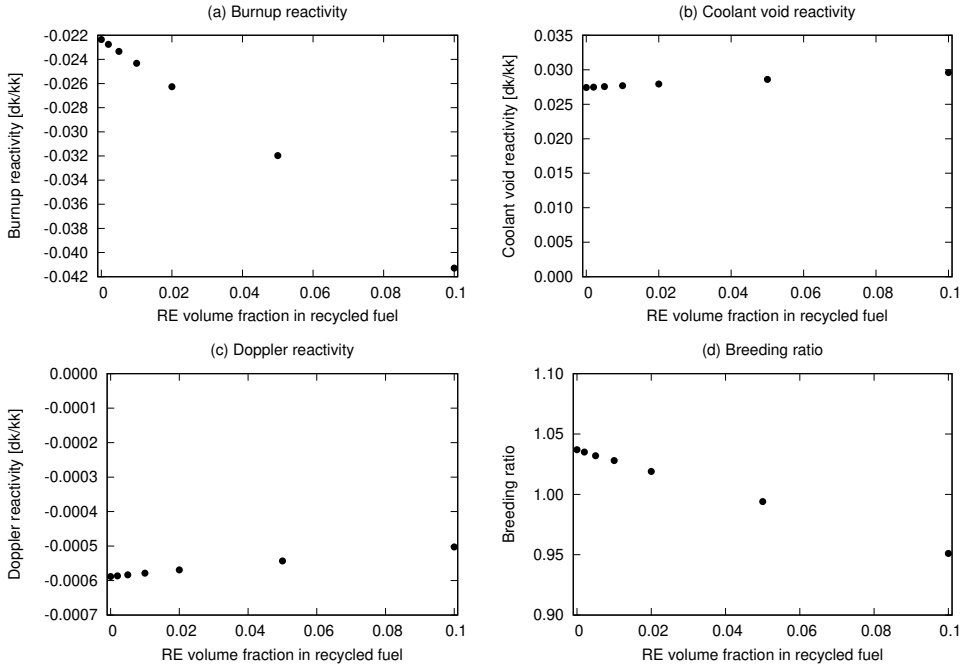

* RE: Rare earth.

Figure 19 Impact of impurities in the recycled fuel on neutronics parameters.

able in FRBurner at present.

The investigation of lattice model effect suggested that the heterogeneous model is crucial for calculation, but the one-dimensional lattice model is sufficiently accurate estimate the neutronic properties. As the heterogeneous models have large influence on k_{eff}, $\Delta\rho_{\text{void}}$ and $\Delta\rho_{\text{Doppler}}$, it is essential to take into account the effect when studying these three parameters with the one-dimensional homogeneous lattice model.

The transport-effect study indicated that the transport solver has a large impact on k_{eff}, and $\Delta\rho_{\text{void}}$ (only for the middle-sized cores). A larger transport-effect on k_{eff} for the fine-energy group calculations means that diffusion theory solver should not be applied with the fine-energy group library. Thus, the use of methodology options in combination with the fine-energy group library and the diffusion theory solver should be avoided. The transport-effect investigation also indicates that diffusion approximation may cause larger bias for sodium-cooled fast reactor system, especially for system which has multiple core

regions.Therefore, when diffusion theory is used in sodium-coolant fast reactor analysis, more attention should be paid on bias. In addition, the study on $P_N S_N$ order of the transport solver revealed that the P_1S_4 option is sufficiently accurate to represent P_3S_8 for a problem which does not require a highly accurate calculation in the preliminary/initial stage.

The fine-energy group effect research demonstrated that the fine-energy group structure calculation is necessary for reasonably accurate analysis of k_{eff}. Considering the magnitude of biases, it is not necessary to apply the fine-energy group calculation for reasonably accurate analysis of β_{eff}, $\Delta\rho_{\text{void}}$ and $\Delta\rho_{\text{Doppler}}$.

Comprehensive investigation of the above-mentioned effects while applying diverse methodologies may be useful in choosing an appropriate methodology for work with a different purpose.

Thirdly, the availability of the detailed burnup chain model was confirmed through numerical calculation using a 197 nuclide detailed chain model on the JSFR-1500 core concept.

Our future works regarding the FRBurner module include the implementation of three dimensional core calculation capability, library generation from the recent libraries, ENDF/B-VIII.0[18] and JEFF-3.3[19], and implementation of the advanced leakage theory[20].

Acknowledgement

This work was supported by *MEXT Innovative Nuclear Research and Development Program*. Grant Number: JPMXDO219209423.

References

[1] Chiba G, Endo T. Numerical benchmark problem of solid-moderated enriched-U-loaded core at Kyoto university critical assembly. J Nucl Sci Technol. 2019; 57:187-195.

[2] Toppel BJ. The Fuel Cycle Analysis Capability REBUS-3. Argonne National Laboratory; 1983.

[3] Rimpault G, Plisson D, Tommasi J, Jacqmin R, RIEUNIER J, VERRIER D, BIRON D. The ERANOS Code and data system for fast reactor neutronic analyses. PHYSOR 2002 - International Conference on the New Frontiers of Nuclear Technology: Reactor Physics, Safety and High-Performance Computing; 2002.

[4] Yokoyama K, Tatsumi M, Hirai Y, Hyoudou H, Numata K, Iwai T, Jin T, Hazama T, Nagaya Y, Chiba G, Kugo T, Ishikawa M. Development of the Next Generation Reactor Analysis Code System, MARBLE. Japan Atomic Energy Agency; 2011.

[5] Stauff NE, Kim TK, Taiwo TA, Buiron L, Rimpault G, Brun E, Lee YK, Pataki I, Kereszturi A, Tota A, Parisi C, Fridman E, Guilliard N, Kugo T, Sugino K, Uematsu MM, Ponomarev A, Messaoudi N, Lin Tan R, Kozlowski T, Bernnat W, Blanchet D, Monti S, Yamaji A, Nakahara Y, Gulliford J. Benchmark for Neutronic Analysis of Sodium-cooled Fast Reactor Cores with Various Fuel Types and Core Sizes. Nuclear Energy Agency of the OECD (NEA); 2016, NEA-NSC-R–2015-9.

[6] MacFarlane RE. NJOY99.0: code system for producing pointwise and multigroup neutron and photon cross sections from ENDF/B data. Los Alamos National Laboratory; 1999.

[7] Tada K, Nagaya Y, Kunieda S, Suyama K, Fukahori T. Development and verification of a new nuclear data processing system FRENDY. J Nucl Sci Technol. 2017; 54:806-817.

[8] Tone T. A numerical study of heterogeneity effects in fast reactor critical assemblies. J Nucl Sci Technol. 1975; 12:467-481.

[9] Kawamoto Y, Chiba G, Tsuji M, et al. Numerical solution of matrix exponential in burnup equation using mini-max polynomial approximation. Ann. Nucl. Energy. 2015; 80:219-224.

[10] Chiba G, Ohoka Y, Yamamoto K, et al. Revisiting mini-max polynomial approximation method for nuclear fuel depletion calculations. Proc. Int. Conf. on Math. Comp. Methods Applied to Nucl. Sci. Eng.; 2019 Aug 25-29; Portland (OR).

[11] Shibata K, Iwamoto O, Nakagawa T, Iwamoto N, Ichihara A, Kunieda S, Chiba S, Furukawa K, Otuka N, Ohsawa T, Murata T, Matsunobu H, Zukaran A, Kameda S, Katakura J. JENDL-4.0: A

new library for nuclear science and technology. J Nucl Sci Technol. 2011; 48:1-30.

[12] Santamarina A, Bernard D, Blaise P, Coste M, Courcelle A, Huynh TD, Jouanne C, Leconte P, Litaize O, Mengelle S, Noguère G, Ruggiéri J-M, Sérot O, Tommasi J, Vaglio C, Vidal J-F. The JEFF-3.1.1 Nuclear Data Library. Paris: OECD Publishing;2009, NEA No. 6807, ISBN 978-92-64-99074-6.

[13] Ohki S, Ogawa T, Kobayashi N, et al. FBR core concepts in the FaCT project in Japan. Proc. Int. Conf. on Physics of Reactors; 2008 Sep 14-19; Interlaken (Switzerland).

[14] Okumura K, Kugo T, Kaneko K, et al. SRAC2006: a comprehensive neutronics calculation code system. Japan: Japan Atomic Energy Agency; 2007, JAEA-Data/Code 2007-004.

[15] Katakura J. JENDL FP decay data file 2011 and fission yields data file 2011. Japan: Japan Atomic Energy Agency; 2011, JAEA-Data/Code 2011-025.

[16] Katakura J, Minato F, Ohgama K. Revision of the JENDL FP fission yield data. EPJ Web of Conferences 2016; 111:08004.

[17] Ohki S. Influence of remaining fission products in low-decontaminated fuel on reactor core characteristics. Japan: Japan Nuclear Fuel Cycle Development Institute; 2002, JNC TN9400 2002-066. (in Japanese)

[18] Brown DA, Chadwick MB, Capote R, Kahler AC, Trkov A, Herman MW, Sonzogni AA, Danon A, Carlson AD, Dunn M, Smith DL, Hale GM, Arbanas G, Arcilla R, Bates CR, Beck B, Becker B, Brown F, Casperson RJ, Conlin J, Cullen DE, Descalle M-A, Firestone R, Gaines T, Guber KH, Hawari AI, Holmes J, Johnson TD, Kawano T, Kiedrowski BC, Koning AJ, Kopecky S, Leal L, Lestone JP, Lubitz C, Márquez Damián JI, Mattoon CM, McCutchan EA, Mughabghab S, Navratil P, Neudecker D, Nobre G, Noguere G, Paris M, Pigni MT, Plompen AJ, Pritychenko B, Pronyaev VG, Roubtsov D, Rochman D, Romano P, Schillebeeckx P, Simakov S, Sin M, Sirakov I, Sleaford B, Sobes V, Soukhovitskii ES, Stetcu I, Talou P, Thompson I, Van der Marck S, Welser-Sherrill L, Wiarda D, White M, Wormald JL, Wright RQ, Zerkle M, Žerovnik G, Zhu Y. ENDF/B-VIII.0: The 8th Major Release of the Nuclear Reaction Data Library with CIELO-project Cross Sections, New

Standards and Thermal Scattering Data. Nuclear Data Sheets. 2018; Volume 148: pages 1-142. ISSN 0090-3752. https://doi.org/10.1016/j.nds.2018.02.001.

[19] Plompen A, Cabellos O, De Saint Jean C, Fleming M, Algora M, Angelone M, Archier M, Bauge E, Bersillon O, Blokhin A, Cantargi F, Chebboubi A, Diez C, Duarte H, Dupont E, Dyrda J, Erasmus B, Fiorito L, Fischer U, Flammini D, Foligno D, Gilbert M, Granada J, Haeck W, Hambsch F, Helgesson P, Hilaire S, Hill I, Hursin M, Ichou R, Jacqmin R, Jansky B, Jouanne C, Kellett M, Kim D, Kim H, Kodeli I, Koning A, Konobeyev A, Kopecky S, Kos B, Krása A, Leal L, Leclaire N, Leconte P, Lee Y, Leeb H, Litaize O, Majerle M, Márquez Damián J, Michel-Sendis F, Mills R, Morillon B, Noguère G, Pecchia M, Pelloni S, Pereslavtsev P, Perry R, Rochman D, Röhrmoser A, Romain P, Romojaro P, Roubtsov D, Sauvan P, Schillebeeckx P, Schmidt K, Serot O, Simakov S, Sirakov I, Sjöstrand H, Stankovskiy A, Sublet J, Tamagno P, Trkov A, Van der Marck S, Velarde F, Villari R, Yokoyama K, Žerovnik G. The joint evaluated fission and fusion nuclear data library, JEFF-3.3. Eur. Phys. J. 2020; A56:181. ISSN 1434-6001 (online).

[20] Van Rooijen W, Chiba G. Diffusion coefficients for LMFBR cells calculated with MOC and Monte Carlo methods. Ann. Nucl. Energy. 2011; 38:133–144

Appendix: Detailed data of FRBurner calculation on four cores with various methodologies

In the following tables, 'JDL/JEF' represents the JENDL-4.0/JEFF-3.1.1, respectively. '70g/280g' means the energy group structure. '0D/1D/2D' represents the lattice model type. 'Di/Tr' means the theory in the whole-core calculation step. 'Yield', 'Absorp', 'Scatt', 'N-leak', 'Leak' and 'Tot $\Delta\rho_{\mathrm{void}}$' represent the yield, absorption, scattering, non-leakage, leakage component of $\Delta\rho_{\mathrm{void}}$ and total $\Delta\rho_{\mathrm{void}}$, respectively.

Table A·1 Original data of FRBurner calculations with various methodologies: MET-1000.

	k_{eff}	β_{eff}	Yield	Absorp	Scatt	N-leak	Leak	Tot $\Delta\rho_{\text{void}}$	$\Delta\rho_{\text{Doppler}}$
The unit of each parameter in this table is per cent mile (PCM) except k_{eff}									
JDL-70g-0D-Di BOEC	1.01403	337	-14	222	3903	4111	-1843	2268	-341
JDL-70g-0D-Di EOEC	0.99501	336	-15	231	4025	4240	-1884	2356	-352
JDL-70g-0D-Tr BOEC	1.01885	337	-14	221	3922	4129	-1812	2317	-339
JDL-70g-0D-Tr EOEC	0.99978	336	-15	229	4046	4260	-1855	2406	-350
JDL-70g-1D-Di BOEC	1.01802	338	-66	199	3856	3988	-1838	2150	-357
JDL-70g-1D-Di EOEC	0.99837	337	-66	205	3978	4116	-1881	2235	-370
JDL-70g-1D-Tr BOEC	1.02284	337	-66	198	3874	4006	-1807	2200	-355
JDL-70g-1D-Tr EOEC	1.00314	336	-66	205	3998	4137	-1851	2286	-367
JDL-70g-2D-Di BOEC	1.01848	338	-73	206	3852	3984	-1838	2146	-356
JDL-70g-2D-Di EOEC	0.99881	337	-73	213	3973	4112	-1881	2231	-369
JDL-70g-2D-Tr BOEC	1.02330	338	-72	206	3869	4002	-1807	2196	354
JDL-70g-2D-Tr EOEC	1.00358	336	-72	212	3993	4133	-1850	2282	-366
JDL-280g-0D-Di BOEC	1.01658	336	-13	219	3827	4033	-1842	2191	-336
JDL-280g-0D-Di EOEC	0.99624	335	-13	228	3953	4168	-1884	2284	-348
JDL-280g-0D-Tr BOEC	1.02459	335	-13	217	3832	4036	-1767	2269	-337
JDL-280g-0D-Tr EOEC	1.00425	334	-14	225	3962	4174	-1810	2364	-349
JDL-280g-1D-Di BOEC	1.02058	336	-80	216	3775	3909	-1837	2072	-352
JDL-280g-1D-Di EOEC	0.99968	335	-81	224	3901	4043	-1881	2162	-365
JDL-280g-1D-Tr BOEC	1.02863	336	-79	213	3781	3915	-1761	2154	-352
JDL-280g-1D-Tr EOEC	1.00772	335	-79	220	3910	4051	-1805	2246	-366
JDL-280g-2D-Di BOEC	1.02104	336	-91	225	3769	3902	-1837	2065	-352
JDL-280g-2D-Di EOEC	1.00011	335	-91	233	3895	4035	-1881	2154	-365
JDL-280g-2D-Tr BOEC	1.02910	336	-90	222	3776	3908	-1761	2147	-352
JDL-280g-2D-Tr EOEC	1.00815	335	-90	229	3905	4044	-1805	2239	-366
JEF-70g-0D-Di BOEC	1.02238	344	-14	210	3777	3972	-1875	2098	-334
JEF-70g-0D-Di EOEC	1.00149	343	-15	219	3903	4107	-1917	2190	-346
JEF-70g-0D-Tr BOEC	1.02729	344	-14	208	3796	3990	-1845	2146	-331
JEF-70g-0D-Tr EOEC	1.00635	343	-14	217	3925	4127	-1888	2240	-344
JEF-70g-1D-Di BOEC	1.02623	345	-50	179	3729	3858	-1870	1988	-350
JEF-70g-1D-Di EOEC	1.00475	343	-50	186	3856	3991	-1913	2078	-364
JEF-70g-1D-Tr BOEC	1.03115	345	-50	179	3747	3876	-1838	2038	-347
JEF-70g-1D-Tr EOEC	1.00960	343	-49	185	3876	4011	-1883	2128	-361
JEF-70g-2D-Di BOEC	1.02666	345	-54	185	3724	3855	-1869	1985	-349
JEF-70g-2D-Di EOEC	1.00516	343	-54	192	3851	3988	-1913	2075	-363
JEF-70g-2D-Tr BOEC	1.03158	345	-54	185	3742	3873	-1838	2035	-346
JEF-70g-2D-Tr EOEC	1.01002	343	-54	192	3871	4009	-1883	2126	-361
JEF-280g-0D-Di BOEC	1.02496	343	-13	209	3699	3896	-1863	2033	-331
JEF-280g-0D-Di EOEC	1.00272	342	-13	219	3830	4036	-1906	2129	-345
JEF-280g-0D-Tr BOEC	1.03401	343	-13	207	3707	3901	-1777	2124	-332
JEF-280g-0D-Tr EOEC	1.01175	341	-14	216	3841	4043	-1820	2223	-346
JEF-280g-1D-Di BOEC	1.02881	343	-62	192	3652	3780	-1858	1922	-347
JEF-280g-1D-Di EOEC	1.00604	342	-62	199	3782	3918	-1903	2015	-362
JEF-280g-1D-Tr BOEC	1.03792	343	-61	190	3659	3788	-1770	2018	-348
JEF-280g-1D-Tr EOEC	1.01512	342	-61	197	3793	3928	-1815	2113	-364
JEF-280g-2D-Di BOEC	1.02926	343	-70	199	3646	3774	-1858	1916	-347
JEF-280g-2D-Di EOEC	1.00646	342	-71	207	3776	3912	-1903	2009	-363
JEF-280g-2D-Tr BOEC	1.03836	343	-69	197	3654	3782	-1770	2012	-348
JEF-280g-2D-Tr EOEC	1.01553	342	-69	205	3787	3922	-1815	2108	-364

Table A·2 Original data of FRBurner calculations with various methodologies: MOX-1000.

	k_{eff}	β_{eff}	Yield	Absorp	Scatt	N-leak	Leak	Tot $\Delta\rho_{\text{void}}$	$\Delta\rho_{\text{Doppler}}$
The unit of each parameter in this table is per cent mile (PCM) except k_{eff}									
JEF-70g-0D-Di BOEC	1.02495	335	-23	408	2842	3226	-1226	2000	-673
JEF-70g-0D-Di EOEC	1.01271	333	-24	417	2889	3283	-1245	2037	-685
JEF-70g-0D-Tr BOEC	1.02844	335	-23	402	2855	3234	-1227	2007	-671
JEF-70g-0D-Tr EOEC	1.01616	333	-24	412	2903	3291	-1248	2043	-683
JEF-70g-1D-Di BOEC	1.02964	336	-86	376	2788	3076	-1225	1851	-707
JEF-70g-1D-Di EOEC	1.01661	333	-88	385	2836	3133	-1246	1886	-721
JEF-70g-1D-Tr BOEC	1.03313	335	-84	369	2800	3085	-1227	1859	-704
JEF-70g-1D-Tr EOEC	1.02006	333	-85	379	2849	3142	-1249	1894	-718
JEF-70g-2D-Di BOEC	1.03000	336	-80	383	2778	3079	-1226	1854	-706
JEF-70g-2D-Di EOEC	1.01697	334	-81	392	2825	3136	-1247	1889	-720
JEF-70g-2D-Tr BOEC	1.03350	335	-78	376	2790	3088	-1227	1862	-703
JEF-70g-2D-Tr EOEC	1.02043	333	-79	386	2838	3145	-1249	1897	-717
JEF-280g-0D-Di BOEC	1.02662	334	-22	430	2765	3173	-1209	1963	-699
JEF-280g-0D-Di EOEC	1.01378	331	-23	441	2813	3231	-1230	2001	-712
JEF-280g-0D-Tr BOEC	1.03277	333	-22	420	2777	3174	-1175	1999	-697
JEF-280g-0D-Tr EOEC	1.01986	331	-23	431	2826	3234	-1196	2038	-711
JEF-280g-1D-Di BOEC	1.03136	334	-125	426	2719	3019	-1211	1808	-733
JEF-280g-1D-Di EOEC	1.01777	332	-127	437	2767	3077	-1233	1844	-749
JEF-280g-1D-Tr BOEC	1.03756	334	-121	415	2730	3024	-1176	1848	-731
JEF-280g-1D-Tr EOEC	1.02389	332	-123	426	2780	3083	-1198	1885	-747
JEF-280g-2D-Di BOEC	1.03172	334	-122	432	2707	3017	-1212	1804	-733
JEF-280g-2D-Di EOEC	1.01810	332	-124	444	2755	3074	-1234	1840	-749
JEF-280g-2D-Tr BOEC	1.03792	334	-119	422	2719	3021	-1177	1845	-731
JEF-280g-2D-Tr EOEC	1.02422	332	-121	433	2768	3080	-1199	1881	-747

Table A·3 Original data of FRBurner calculations with various methodologies: MOX-3600.

	k_{eff}	β_{eff}	Yield	Absorp	Scatt	N-leak	Leak	Tot $\Delta\rho_{\text{void}}$	$\Delta\rho_{\text{Doppler}}$
The unit of each parameter in this table is per cent mile (PCM) except k_{eff}									
JDL-70g-0D-Di BOEC	0.99755	363	-18	424	2462	2868	-639	2229	-862
JDL-70g-0D-Di EOEC	1.00670	354	-18	409	2475	2866	-626	2240	-816
JDL-70g-0D-Tr BOEC	1.00088	362	-17	419	2474	2876	-655	2221	-858
JDL-70g-0D-Tr EOEC	1.01009	354	-17	404	2487	2874	-641	2233	-812
JDL-70g-1D-Di BOEC	1.00313	363	-100	382	2401	2681	-640	2042	-907
JDL-70g-1D-Di EOEC	1.01069	355	-100	373	2420	2691	-627	2064	-861
JDL-70g-1D-Tr BOEC	1.00646	363	-97	376	2411	2690	-655	2036	-903
JDL-70g-1D-Tr EOEC	1.01408	355	-97	366	2431	2700	-642	2058	-857
JDL-70g-2D-Di BOEC	1.00326	363	-95	394	2394	2692	-640	2053	-903
JDL-70g-2D-Di EOEC	1.01089	355	-95	383	2414	2702	-627	2074	-857
JDL-70g-2D-Tr BOEC	1.00659	363	-92	387	2405	2701	-655	2046	-899
JDL-70g-0D-Tr EOEC	1.01428	355	-92	377	2425	2710	-642	2068	-853
JDL-280g-0D-Di BOEC	0.99872	361	-17	441	2394	2818	-637	2181	-884
JDL-280g-0D-Di EOEC	1.00732	352	-17	426	2411	2820	-624	2196	-838
JDL-280g-0D-Di BOEC	1.00313	361	-17	433	2406	2822	-641	2181	-882
JDL-280g-0D-Di EOEC	1.01175	352	-16	418	2423	2824	-628	2196	-836
JDL-280g-0D-Di BOEC	1.00432	362	-164	484	2313	2633	-638	1994	-929
JDL-280g-0D-Di EOEC	1.01138	353	-163	471	2338	2646	-627	2019	-883
JDL-280g-0D-Di BOEC	1.00876	361	-158	465	2331	2639	-642	1997	-927
JDL-280g-0D-Di EOEC	1.01585	353	-157	453	2356	2652	-630	2022	-881
JDL-280g-0D-Di BOEC	1.00445	362	-156	476	2319	2639	-639	1999	-927
JDL-280g-0D-Di EOEC	1.01155	353	-155	464	2344	2651	-627	2024	-880
JDL-280g-0D-Di BOEC	1.00889	361	-151	461	2335	2645	-642	2002	-924
JDL-280g-0D-Di EOEC	1.01602	353	-150	449	2359	2658	-631	2027	-878
JEF-70g-0D-Di BOEC	1.00339	371	-19	416	2321	2718	-648	2071	-860
JEF-70g-0D-Di EOEC	1.00964	362	-19	403	2352	2736	-635	2102	-818
JEF-70g-0D-Di BOEC	1.00676	371	-18	410	2331	2724	-664	2059	-856
JEF-70g-0D-Di EOEC	1.01307	362	-18	397	2362	2742	-651	2090	-814
JEF-70g-0D-Di BOEC	1.00880	372	-92	369	2264	2540	-647	1892	-906
JEF-70g-0D-Di EOEC	1.01351	363	-93	361	2300	2567	-636	1931	-864
JEF-70g-0D-Di BOEC	1.01218	372	-88	362	2272	2546	-664	1882	-902
JEF-70g-0D-Di EOEC	1.01694	363	-89	354	2309	2574	-653	1921	-860
JEF-70g-0D-Di BOEC	1.00890	372	-85	380	2257	2552	-648	1904	-902
JEF-70g-0D-Di EOEC	1.01368	363	-86	371	2294	2579	-636	1943	-860
JEF-70g-0D-Di BOEC	1.01227	372	-82	373	2266	2558	-664	1894	-898
JEF-70g-0D-Di EOEC	1.01710	363	-82	365	2303	2585	-652	1933	-856
JEF-70g-0D-Di BOEC	1.00441	370	-18	435	2255	2672	-645	2027	-884
JEF-70g-0D-Di EOEC	1.01010	361	-18	421	2289	2693	-632	2061	-842
JEF-70g-0D-Di BOEC	1.00899	369	-17	426	2265	2674	-648	2025	-882
JEF-70g-0D-Di EOEC	1.01470	361	-17	413	2299	2695	-636	2058	-582
JEF-70g-0D-Di BOEC	1.00983	370	-150	445	2199	2494	-646	1848	-931
JEF-70g-0D-Di EOEC	1.01404	362	-150	435	2240	2524	-635	1889	-889
JEF-70g-0D-Di BOEC	1.01444	370	-144	432	2210	2498	-649	1849	-928
JEF-70g-0D-Di EOEC	1.01867	361	-145	422	2250	2528	-638	1890	-887
JEF-70g-0D-Di BOEC	1.00993	370	-141	445	2198	2501	-646	1855	-928
JEF-70g-0D-Di EOEC	1.01418	362	-141	435	2238	2531	-635	1896	-886
JEF-70g-0D-Di BOEC	1.01454	370	-136	433	2208	2505	-649	1856	-926
JEF-70g-0D-Di EOEC	1.01881	362	-136	423	2248	2535	-639	1896	-884

Table A·4 Original data of FRBurner calculations with various methodologies: CAR-3600.

	k_{eff}	β_{eff}	Yield	Absorp	Scatt	N-leak	Leak	Tot $\Delta\rho_{\text{void}}$	$\Delta\rho_{\text{Doppler}}$
The unit of each parameter in this table is per cent mile (PCM) except k_{eff}									
JEF-70g-0D-Di BOEC	0.99739	381	-20	478	2721	3179	-860	2319	-911
JEF-70g-0D-Di EOEC	1.01143	371	-18	456	2781	3219	-797	2423	-859
JEF-70g-0D-Tr BOEC	0.99988	381	-19	467	2734	3182	-874	2308	-907
JEF-70g-0D-Tr EOEC	1.01402	371	-18	446	2794	3222	-817	2405	-856
JEF-70g-1D-Di BOEC	1.00288	382	-90	425	2651	2985	-857	2128	-955
JEF-70g-1D-Di EOEC	1.01528	372	-90	411	2719	3039	-798	2241	-904
JEF-70g-1D-Tr BOEC	1.00537	381	-84	412	2662	2990	-871	2118	-952
JEF-70g-1D-Tr EOEC	1.01786	372	-84	398	2729	3042	-817	2225	-901
JEF-70g-2D-Di BOEC	1.00315	382	-81	435	2638	2991	-857	2134	-952
JEF-70g-2D-Di EOEC	1.01557	372	-81	420	2706	3044	-798	2246	-901
JEF-70g-2D-Tr BOEC	1.00563	382	-76	422	2649	2995	-871	2124	-949
JEF-70g-2D-Tr EOEC	1.01815	372	-76	407	2717	3047	-817	2230	-898
JEF-280g-0D-Di BOEC	0.99930	380	-18	498	2617	3097	-853	2243	-930
JEF-280g-0D-Di EOEC	1.01260	370	-17	476	2680	3139	-792	2347	-880
JEF-280g-0D-Tr BOEC	1.00325	379	-18	482	2629	3093	-851	2242	-928
JEF-280g-0D-Tr EOEC	1.01631	370	-17	460	2692	3136	-795	2341	-879
JEF-280g-1D-Di BOEC	1.00478	380	-147	509	2543	2904	-853	2051	-974
JEF-280g-1D-Di EOEC	1.01649	371	-145	489	2616	2959	-794	2165	-924
JEF-70g-1D-Tr BOEC	1.00875	380	-137	484	2556	2903	-850	2053	-971
JEF-70g-1D-Tr EOEC	1.02023	371	-135	465	2629	2959	-797	2162	-922
JEF-70g-2D-Tr BOEC	1.00505	380	-137	508	2534	2904	-853	2051	-972
JEF-70g-2D-Tr EOEC	1.01676	371	-136	490	2607	2960	-795	2165	-922
JEF-70g-2D-Tr BOEC	1.00903	380	-129	485	2548	2903	-850	2053	-970
JEF-70g-2D-Tr EOEC	1.02050	371	-128	467	2620	2959	-797	2162	-921

Table A·5 Burnup reactivity $\Delta\rho_{\text{cycle}}$ given by different references (unit: pcm)

	MET-1000	MOX-1000	MOX-3600	CAR-3600
ANL-1	-1897	-1010	661	1519
CEA-1	-2594	-1672	-253	486
CEA-10	-2572	-1874	-256	484
CER	-1471	-537	1400	2532
JAEA-2	-2004	/	574	/
KIT	-2322	-1598	26	/
UIUC-3	-2103	-1731	69	723
IKE-1	-2719	/	/	/
Average	-2210	-1443	312	1149
(±SD)	422	483	542	882